Formation of organic molecular nanocrystals under rigid confinement with analysis by solid state NMR

Citation: Yang, X. et al. "Formation of Organic Molecular Nanocrystals under Rigid Confinement with Analysis by Solid State NMR." CrystEngComm 16.39 (2014): 9345–9352.

As Published: http://dx.doi.org/10.1039/c4ce01087f

Publisher: Royal Society of Chemistry

Persistent URL: http://hdl.handle.net/1721.1/105135

Version: Author's final manuscript: final author's manuscript post peer review, without publisher's formatting or copy editing

Published in final edited form as:
CrystEngComm. 2014 October 21; 16(39): 9345–9352. doi:10.1039/C4CE01087F.

Formation of Organic Molecular Nanocrystals under Rigid Confinement with Analysis by Solid State NMR

X. Yang[a], **T. C. Ong**[b], **V. K. Michaelis**[b], **S. Heng**[a], **J. Huang**[a], **R. G. Griffin**[b], and **A. S. Myerson**[a]

[a]Department of Chemical Engineering, Massachusetts Institute of Technology, 77 Massachusetts Avenue, Cambridge, MA 02139, USA

[b]Department of Chemistry and Francis Bitter Magnet Laboratory, Massachusetts Institute of Technology, 77 Massachusetts Avenue, Cambridge, MA 02139, USA

Abstract

Crystallization in rigid confinement is a promising method to obtain organic molecular nanocrystals. However, the crystallization behavior and the related characterization methods are not well studied. Here we present a systematic study of the nucleation of organic molecular nanocrystals in rigid pores. Four different compounds were studied, ibuprofen, fenofibrate, griseofulvin, and indomethacin, which range from simple to complex molecules. Solid-state Nuclear Magnetic Resonance (NMR) was employed to analyse the structure of these compounds inside pores which are difficult to characterize by other analytical methods. We successfully demonstrated the production of nano-crystalline ibuprofen, fenofibrate and griseofulvin in porous silica particles with ~ 40 nm pores. These nanocrystals showed significant enhancement in dissolution rates. These results help advance the fundamental understanding of nucleation under rigid confinement and may lead to potential applications in developing new formulations in the pharmaceutical industry.

1 Introduction

The formation of organic molecular nanocrystals is a topic of great interest in the pharmaceutical industry because of the potential increase in solubility and dissolution rate of organic molecular crystals below 1 μm[1–4]. Direct production of nanocrystals through crystallization (Bottom-up approach) while controlling the crystal form (polymorph) is a difficult problem and an active area of research[4]. For primary nucleation in nano/pico-sized droplets, classical nucleation theory gives a relation between induction time and volume:

$$induction\ time = \frac{1}{nucleation\ rate * volume}$$

Electronic Supplementary Information (ESI) available: details of dissolution tests and reference XRPD patterns. See DOI: 10.1039/c000000x/

As the droplet size decreases, the induction time may significantly increase if the nucleation rate is assumed constant. Thus attempts to obtain nanocrystals from small volumes often require long induction times or result in amorphous solids. Herefore, among various bottom-up methods, to obtain nanocrystalline materials rather than their amorphous states is still hard. Previous investigators researchers have explored many novel methods for nanocrystal formation such as spray drying[3], supercritical fluid crystallization[5, 6], impinging jets[7, 8], microfluidic devices[9–11] and nano-porous confinement[12–16]. Nano-crystallization in porous materials is considered a promising method because of its relatively simplicity. The porous materials can be generally divided into two categories, soft confinement (mostly polymer) and rigid confinement (mostly inorganic materials, such as porous silica, alumina and zeolite). Here, we mainly focus on the rigid confinement. Previously, Ha et al. examined the polymorphic outcomes of anthranilic acid in 7.5, 24 and 55 nm controlled pore glasses and found that the metastable polymorph (form II) preferably crystallized in smaller pores and remained stabilized for at least one month.[17] Similar results were also reported in the pimelic acid, subric acid, and coumarin systems.[18]

Compounds nanocrystallized inside porous matrices can be challenging to characterize. Traditional crystallographic techniques such as x-ray powder diffraction (XRPD) rely on diffraction of incident x-ray off the sample surface, which becomes difficult if the nanocrystals are embedded within the pores and of low concentration. Solid-state NMR (ssNMR), which is not constrained in this way, is therefore a viable method to study nano-crystallization in compatible porous systems.[19] Combined with magic angle spinning (MAS) and cross polarization (CP) at high magnetic fields (≥ 11.7 T), solid-state NMR offers high resolution for studies of various polymorphs, hydrates, and solvates.[20, 21] NMR parameters such as chemical shift, linewidths, and relaxation are sensitive to polymorphism and crystallinity,[22–26] and in recent years more advanced NMR techniques have been applied for structural and dynamics studies of pharmaceuticals.[27, 28] In one study, Lubach et al. examined by ^{13}C CPMAS NMR bupivacaine, a local anesthetic, encapsulated in lipospheres in tristearin/protein matrix.[29] In another study, Azaïs et al. investigated ibuprofen embedded in the mesoporous silica particle MCM-41,[30] whereas they characterized the system by a combination of ^{1}H, ^{13}C, and ^{29}Si MAS NMR and evaluated the impact of temperature (218 – 286 K) and pore diameters (35 and 116 Å). They found that ibuprofen exhibits liquid-like molecular dynamics inside the pores at room temperature, with higher mobility associated with the larger pore size. Recently, dynamic nuclear polarization, which can improve NMR signal-to-noise by factors of 10^2–10^3, has been applied to porous materials[31–34] and pharmaceutical samples,[35, 36] so the technique may prove useful for NMR studies of organic molecular nanocrystals embedded in porous matrices.

This work aims to develop a novel formulation method to produce nano-sized organic molecular nanocrystals while controlling the polymorphic outcome under rigid confinement. To this end, four different organic compounds were selected as model compounds as shown in Figure 1: ibuprofen (IBP), fenofibrate (FEN), griseofulvin (GSF) and indomethacin (IMC). Biocompatible porous silica particles were used as the porous matrices. Experimental conditions such as evaporation rates and loading percentages were tuned to better control the polymorphic outcome and nucleation rate. Information on the crystallinity and crystalline forms obtained are analysed by solid-state NMR. We anticipate that our

results will help improve the fundamental understanding of nucleation and polymorphism of nanocrystals under rigid confinement and lead to novel formulation methods in industry.

2 Experimental Section

2.1 Materials

Ibuprofen, fenofibrate, griseofulvin and indomethacin were obtained from Sigma Aldrich. Silicon dioxide (silica) particles of ~ 40 nm pores (AEROPERL® 300 Pharma, bead-like mesoporous granules with 37 μm particle size) were obtained from Evonik USA. Silica particles of ~ 10 nm pores were obtained from EPRUI Nanoparticles & Microspheres Co. Ltd.

2.2 Experimental set-up (Figure 2)

(1) Undersaturated active pharmaceutical ingredient (API) solutions were prepared (i.e. 5 g IBP in 10 ml ethanol). A given amount of porous silica particles were weighed (i.e., 1 g of silica particles, AEROPERL®, pore size ~40 nm) and put into a 50 ml Buchner flask (the silica particles were pre-washed/dried with the solvent used to make the API solutions). A rubber cap was used to seal the Buchner flask. The Buchner flask was then connected to a vacuum line (~ 0.5 atm) in order to prevent possible trapping of air inside pores during the loading process. (2) After 10 minutes, API solution was filled in a syringe with a needle, and then injected into the Buchner flask through the rubber cap. To enhance the mass transfer, the flask was lightly shaken for the silica particles to be suspended and then kept still for 60 minutes. (3) Afterwards, a filtration and washing step was applied to remove adhering solution from the surface of these particles. (4) The particles were then taken into different experimental chambers for controlled crystallization processes. Various crystallization methods (slow evaporation, slow cooling and anti-solvent methods) were evaluated and slow evaporation was chosen as the major method since it is easy to control and to perform multiple experiments. The crystallization time was a minimum of 12 hours. (5) Samples were also put into a vacuum oven overnight to evaporate all residual solvents before analysis, but no significant loss of mass was observed. For each experimental data point, samples of control group (these five steps are also performed for samples with pure solvent) were measured the weight increase as well, and were found to lose 0 ~ 2 wt% due to adhered silica particles onto walls of Buchner flasks.

2.3 X-Ray Powder Diffraction (XRPD) analysis

All powdered products were identified using a PANalytical X'Pert PRO diffractometer using 45 kV and an anode current of 40 mA. The instrument is equipped with a PW3050/60 standard resolution goniometer and a PW3373/10 Cu LFF DK241245 X-ray tube. Samples were prepared on placed on a spinner sample stage (PW3064, Reflection mode). Settings on incident beam path include: soller slit 0.04 rad., mask fixed 10 mm, programmable divergence slit and fixed 1° anti-scatter slit. Settings on diffracted beam path include: soller slit 0.04 rad. and programmable anti-scatter slit. The scan was programmed as a continuous scan: 2θ angle 2 ~ 40°, step size 0.0083556°, time per step 19.685 s; three repeated scans were collected to average.

2.4 Differential Scanning Calorimetry (DSC) analysis

The instrument (Q2000, TA instruments) is connected with a nitrogen gas cylinder to maintain a flow rate of 50 ml/min in order to create an inert gas environment in the sample chamber. An extra refrigerated cooling system (RCS 40, TA instruments) is used to extend the available temperature range to −40 ~ 400 °C. Tzero® pan and lid were used. A heating/cooling rate of 5 °C/min was applied and different initial/final temperatures were set for different compounds.

2.5 Solid-state Nuclear Magnetic Resonance (ssNMR) method

Solid-state NMR experiments were conducted on a home-built 500 MHz spectrometer (courtesy of Dr. Dave Ruben, FBML) using either a 3.2 mm or a 4 mm Varian triple resonance ($^{1}H/^{13}C/^{15}N$) probe. For the CPMAS experiments,[37] the CP contact time was 2.0 ms at ν_{rf} of 83 kHz and the MAS frequency was between 10 to 13.5 kHz. The ^{1}H T_1 was measured either by the inversion-recovery38 or the saturation recovery[39] sequence. All experiments utilized the two pulse phase modulation (TPPM)[40] proton decoupling sequence. The recycling time for all samples was 5 s. The number of scans was up to 80,000 depending on the signal to noise. The spectrometer was referenced to adamantane (40.49 ppm) with respect to DSS (0 ppm). Quantification of API polymorphs from CPMAS spectra was performed following the procedure published by Offerdahl et al.[22]

2.6 Dissolution test

The dissolution tests follow the USP standards. Analysis of concentration used either High-Performance Liquid Chromatography (HPLC) or ultraviolet–visible spectroscopy (UV-Vis) (Details can be found in SI). Here, we take IBP as an example to describe the procedure. The dissolution medium used for IBP was a pH 7.2 phosphate buffer. The phosphate buffer was made using monobasic potassium phosphate, sodium hydroxide, and water. 27.22 grams of potassium phosphate was weighed out and dissolved in 1000 mL of water. 50 mL of the solution was mixed with 34.7 mL of 0.2 M sodium hydroxide solution, and water was added to form 200 mL of the phosphate buffer. The dissolution profile of the sample was determined using the USP Dissolution Apparatus 2 at 37 °C. The apparatus operated under 50 revolutions per minute. 900 mL of the dissolution medium was allowed to reach temperature equilibrium before the sample was placed in the medium. Approximately 1.0 mL of the mixture was taken out and filtered each time for a concentration test. The percentage of IBP dissolved in the medium was determined using high-performance liquid chromatography (HPLC). The mobile phase for the HPLC was made using chloroacetic acid, acetonitrile, and water. 4.0 g of chloroacetic acid was weighed out and dissolved in 400 g of water. The solution was then mixed with 600 mL of acetonitrile and degassed. A sample of the control group was prepared using a physical mixture of the same weights of porous silica particles and the compound bulk crystals as the sample tested.

3 Results and discussion

Ibuprofen (IBP), griseofulvin (GSF), fenofibrate (FEN) and indomethacin (IMC) were selected as model compounds to represent APIs from simple to complex. IBP has two known polymorphs (I and II), but the second polymorph has only benn produced in a small

account (milligrams) with a complicated heating/quenching loop.[41] GSF has three different polymorphs (I/II/III) with form I the most stable form.[42] FEN possesses two different polymorphs (I/II, stability: form I > form II).[43] IMC was reported to have eight different polymorphs: the most stable form is γ-form and the metastable form often produced is α-form.[44]

All loading masses and experimental data from XRPD, DSC and ssNMR on the four compounds are summarized in Table 1–4. Each number with an error bar represents at least 10 experimental data points. In preliminary tests we found that we were unable to crystallize IBP in porous silica particles with ~ 10 nm pores and that the release rate from the pores was slow and likely limited by the rate of diffusion. Based on this result we focused our work on porous silica particles with ~ 40 nm pores.

One of the major challenges in this work is to demonstrate that the compounds are successfully loaded inside the porous matrices rather than on the external surfaces. We thus examined the role of washing by varying washing intensity and then using various analytical techniques to characterize these samples. Optical and scanning electronic microscopy was used to check whether any obvious crystals can be seen on the external surfaces of particles. XRPD is very sensitive to surface crystals. DSC is able to detect the melting point depression of nanocrystals (since crystals inside pores are constrained by pore dimensions). Solid state NMR analysis may show the existence of amorphous/crystalline materials and their quantitative amounts.

3.1 Importance of washing

A study of loading amounts vs. washing intensities was performed on IBP. Table 1 shows results of IBP loaded inside porous silica particles with different washing levels. Cold pure solvent (~ 4 °C) was used as the washing solvent after the filtration step. The washing levels were quantified by the volume of cold solvent used. However, it is difficult to ensure that every particle was washed and every sample was washed exactly the same way. Solution residue is left on the surface of the particles if washing is not sufficient, and bulk surface crystals may form during crystallization. The results indicate that the loading of compounds into the porous particles is significantly impacted by the washing employed. As confirmed by optical microscope and XRPD (see discussions below), medium- and strong-wash IBP, strong-wash FEN, strong-wash GSF, strong-wash IMC samples all showed a significant loading amounts without surface crystals, which suggests that compounds were successfully loaded into the pores.

3.2 Surface crystals: optical microscope and XRPD analysis

In Table 1, IBP Samples without washing exhibit an average loading of 28.2 wt%. For these samples, a few large surface crystals could be observed under the polarized optical microscope (100X). These surface crystals contribute a major part of signal in the XRPD. The number of X-ray photons into the sample decays exponentially as the depth increases, and therefore the major part of the XRPD pattern represents crystals on the surface and within a few micrometers below the surface. For example, the XRPD patterns as shown in Figure 3 were collected from the samples of light wash and medium wash. The pattern of

samples of light wash exhibits the characteristic peaks of form I while no peaks are present in the pattern of samples of medium wash (SEM image in SI also confirmed no surface crystals). The reason of peak broadening is not due to size reduction of nanocrystals but from non-uniform height differences of silica particles. The results suggest the existence of form I crystals and no crystals on the surface or within a few micrometers below the surface of samples of light- and medium-wash, respectively.

Similar results were also observed for FEN and GSF (Table 2 and 3). As the washing intensity went from light to strong, XRPD analysis were not able to detect any crystalline peaks.

3.3 Melting point depression of nanocrystals by DSC

The presence of surface crystals as compared to crystals inside the pores can also be examined using DSC. Nanocrystals will display melting point depression[13, 18] while crystals present on the surface will not as they will be larger and will correspond to the normal bulk melting point. A typical DSC curve is illustrated in Figure 4, in which FEN samples which were lightly washed show the major peak of 71.4 °C as well as a small peak at 81.2 °C. The small peak indicates the existence of surface bulk crystals since it matches the bulk melting point of FEN (81.4 ± 0.2 °C). The result is consistent with the corresponding XRPD analysis. The major peak (71.4 °C) should be the melting peak of nano-sized crystals of FEN, which were crystallized inside the confined pores. Similar melting behavior was also seen in IBP and GSF (Table 1 and 3).

3.4 Qualitative and quantitative analysis by solid state NMR

Another method, solid-state NMR, was applied to further analyse the nanocrystals under the confinement. As shown in Figure 5 (One IBP sample of medium wash was used for the NMR study), we observed the onset of additional peaks in the aliphatic region of silica-IBP, which suggests IBP polymorphism. The ratio of the two forms is 79:21. The finding of polymorphism is intriguing. Form II of IBP was reported in 2009, but only a small amount was obtained with a very complex heating/quenching method.[41] However, we do not believe the second polymorph observed is form II, as the observed chemical shifts are inconsistent with the NMR spectrum of form II reported in literature.[45] However, no other polymorph of IBP has been reported. If it is not form II, it could be a new polymorph of IBP; although our DSC results do not indicate signs of a second polymorph. It may be due to the melting points being close to form I and therefore indistinguishable. An alternative explanation is the silica base interacting with the IBP drug may induce a distinctive ^{13}C shift; further investigations are currently underway.

A similar combination of polymorphs was also observed in the study of GSF. In the DSC results of light wash GSF samples, we observed glass transitions and recrystallization processes during heating. These characteristics normally indicate the existence of amorphous content in the sample. We conducted ssNMR on one sample to confirm. The CPMAS ^{13}C spectrum of silica-GSF (Figure 6) shows that the sample is a combination of amorphous content and two distinct crystalline polymorphs. DSC results confirmed the existence of a small amount of surface bulk crystals, and XRPD shows characteristic peaks

of the most stable form (form I). Therefore, one of the two polymorphs can be confirmed as form I. We took one strong washed GSF sample to further explore the control of its polymorphic outcome. As shown in the bottom part of Figure 6, only one set of polymorph peaks remains along with the amorphous material. (Complete assignment of peaks is presented in SI, using previously published solution NMR spectra[46, 47]) This finding indicates that the polymorph I formed on the silica surface diminished from the stronger wash while the second polymorph formed inside the silica pores along with the amorphous content were relatively unaffected. XRPD of the strong washed samples show no crystalline peaks, proving no surface crystals remained. The DSC curves exhibit a major broadening endothermic peak at 205.3 °C and a small broadening peak at 215.2 °C. Apparently, the second polymorph is a metastable form but we are not sure it is form II or III. Nevertheless, these results indicate that complex compounds tend to form metastable polymorphs, or even amorphous content under the rigid confinement. Analysis of FEN was relatively simple. FEN was found to be only one form (form I) in the pores (Solid state NMR Spectra of FEN can be found in SI).

The last compound studied was IMC, which was difficult to crystallize. We used the slow evaporation method and allowed up to 14 days for crystallization. However, DSC analysis still showed no peaks while the solid-state NMR confirmed it was 100% amorphous content (Solid state NMR Spectra of IMC can be found in SI). One interesting phenomena we observed for this sample is that the amorphous states are quite stable. We ran the DSC analysis of the samples after one-month storage and still no crystalline peak was detected. Possible reasons for such stable amorphous IMC materials under this condition are: (1) the porous matrices act as blockers for moisture to come in; (2) the confinement limits the movement of molecules to reorganize.

3.5 Enhanced dissolution profile for nanocrystalline materials

Dissolution profiles of these nanocrystals were tested and the results are shown in Figure 7. For IBP, it took only 1 minute to achieve ~ 50% release while the control group needed 6 minutes to reach almost the same percentage. The control group is a physical mixture of porous silica particles and IBP crystals from commercial sources. Similar trends were also seen in FEN, GSF and IMC. These results demonstrate nanocrystals under the rigid confinement can be used as a novel formulation method and will strongly improve the dissolution rates of poorly soluble active pharmaceutical ingredients.

4 Conclusion

In summary, by using nano-crystallization under rigid confinement we successfully obtained nano-crystalline ibuprofen, fenofibrate and griseofulvin. The results of dissolution tests illustrate the significant enhancement of dissolution profiles of those compounds when present in the form of nanocrystals. In the pharmaceutical industry, making amorphous or nano-crystalline materials is a common practice to enhance the bioavailability of poorly soluble drugs. However, it is difficult to stabilize amorphous or nano-crystalline materials in the formulation, especially for a long time. Our method uses the porous matrix to block the diffusion of moisture, limit the reorganization movement of API molecules and therefore

can stabilize the desired state of the APIs. In addition, the process is very simple and the samples can be directly formulated into capsules without further formulation.

Supplementary Material

Refer to Web version on PubMed Central for supplementary material.

Acknowledgments

We thank the Novartis-MIT center for continuous manufacturing for financial support and use of instrumentation. NMR studies were supported by the National Institutes of Health (NIH grant nos. EB-002026, EB-003151, and EB-002804). V.K.M. is grateful to the Natural Sciences and Engineering Research Council of Canada and Government of Canada for a Banting Postdoctoral Fellowship.

Notes and references

1. Merisko-Liversidge EM, Liversidge GG. Toxicologic pathology. 2008; 36:43–48. [PubMed: 18337220]
2. Faraji AH, Wipf P. Bioorganic & medicinal chemistry. 2009; 17:2950–2962. [PubMed: 19299149]
3. Wang M, Rutledge GC, Myerson AS, Trout BL. Journal of pharmaceutical sciences. 2012; 101:1178–1188. [PubMed: 22189503]
4. Kim K, Lee IS, Centrone A, Hatton TA, Myerson AS. Journal of the American Chemical Society. 2009; 131:18212. [PubMed: 19958030]
5. Turk M, Lietzow R. Journal of Supercritical Fluids. 2008; 45:346–355.
6. Reverchon E, Porta GD, Falivene MG. Journal of Supercritical Fluids. 2000; 17:239–248.
7. Siddiqui SW, Zhao Y, Kukukova A, Kresta SM. Ind Eng Chem Res. 2009; 48:7945–7958.
8. Chioua H, Chana HK, Henga D, Prudhommeb RK, Raperc JA. Journal of Aerosol Science. 2008; 39:500–509.
9. Sultana, M. Thesis: Microfluidic Systems for Continuous Crystallization of small organic molecules. Masschusetts Institute of Technology; Cambridge: 2010.
10. Genota V, Desportesb S, Croushorea C, Lefevrea J, Pansua RB, Delairea JA, Rohrb PR. Chemical Engineering Journal. 2010; 161:234–239.
11. Ildefonso M, Candoni N, Veesler S. Crystal Growth & Design. 2013; 13:2107–2110.
12. Hamilton BD, Hillmyer MA, Ward MD. Crystal Growth & Design. 2008; 8:3368–3375.
13. Ha JM, Hillmyer MA, Ward MD. The Journal of Physical Chemistry B. 2005; 109:1392–1399. [PubMed: 16851108]
14. Ha JM, Hamilton BD, Hillmyer MA, Ward MD. Crystal Growth & Design. 2012; 12:4494–4504.
15. Qian KK, Bogner RH. Journal of pharmaceutical sciences. 2012; 101:444–463. [PubMed: 21976048]
16. Maheshwari P, Dutta D, Sharma SK, Sudarshan K, Pujari PK, Majumder M, Pahari B, Bandyopadhyay B, Ghoshray K, Ghoshray A. The Journal of Physical Chemistry C. 2010; 114:4966–4972.
17. Ha JM, Wolf JH, Hillmyer MA, Ward MD. J Am Chem Soc. 2004; 126:3382. [PubMed: 15025439]
18. Ha JM, Hamilton BD, Hillmyer MA, Ward MD. Crystal Growth & Design. 2009; 9:4766–4777.
19. Skorupska E, Jeziorna A, Kazmierski S, Potrzebowski MJ. Solid State Nucl Mag. 2014; 57–58:2–16.
20. Vogt FG. Future Med Chem. 2010; 2:915–921. [PubMed: 21426109]
21. Griffin JM, Martin DR, Brown SP. Angew Chem Int Edit. 2007; 46:8036–8038.
22. Offerdahl TJ, Salsbury JS, Dong ZD, Grant DJW, Schroeder SA, Prakash I, Gorman EM, Barich DH, Munson EJ. J Pharm Sci-Us. 2005; 94:2591–2605.
23. Lubach JW, Xu DW, Segmuller BE, Munson EJ. J Pharm Sci-Us. 2007; 96:777–787.

24. Barich DH, Davis JM, Schieber LJ, Zell MT, Munson EJ. J Pharm Sci-Us. 2006; 95:1586–1594.
25. Masuda K, Tabata S, Kono H, Sakata Y, Hayase T, Yonemochi E, Terada K. Int J Pharm. 2006; 318:146–153. [PubMed: 16675172]
26. Harris RK. Analyst. 2006; 131:351–373. [PubMed: 16496044]
27. Geppi M, Mollica G, Borsacchi S, Veracini CA. Appl Spectrosc Rev. 2008; 43:202–302.
28. Pham TN, Watson SA, Edwards AJ, Chavda M, Clawson JS, Strohmeier M, Vogt FG. Mol Pharmaceut. 2010; 7:1667–1691.
29. Lubach JW, Padden BE, Winslow SL, Salsbury JS, Masters DB, Topp EM, Munson EJ. Anal Bioanal Chem. 2004; 378:1504–1510. [PubMed: 15214410]
30. Azais T, Tourne-Peteilh C, Aussenac F, Baccile N, Coelho C, Devoisselle JM, Babonneau F. Chem Mater. 2006; 18:6382–6390.
31. Rossini AJ, Zagdoun A, Lelli M, Canivet J, Aguado S, Ouari O, Tordo P, Rosay M, Maas WE, Coperet C, Farrusseng D, Emsley L, Lesage A. Angew Chem Int Edit. 2012; 51:123–127.
32. Lesage A, Lelli M, Gajan D, Caporini MA, Vitzthum V, Miéville P, Alauzun J, Roussey A, Thieuleux C, Mehdi A, Bodenhausen G, Coperet C, Emsley L. Journal of the American Chemical Society. 2010; 132:15459–15461. [PubMed: 20831165]
33. Kobayashi T, Lafon O, Lilly Thankamony AS, Slowing II, Kandel K, Carnevale D, Vitzthum V, Vezin H, Amoureux J-P, Bodenhausen G, Pruski M. Physical Chemistry Chemical Physics. 2013; 15:5553–5562. [PubMed: 23459985]
34. Gunther WR, Michaelis VK, Caporini MA, Griffin RG, Román-Leshkov Y. Journal of the American Chemical Society. 2014; 136:6219–6222. [PubMed: 24697321]
35. Ong TC, Mak-Jurkauskas ML, Walish JJ, Michaelis VK, Corzilius B, Smith AA, Clausen AM, Cheetham JC, Swager TM, Griffin RG. J Phys Chem B. 2013; 117:3040–3046. [PubMed: 23421391]
36. Rossini AJ, Widdifield CM, Zagdoun A, Lelli M, Schwarzwalder M, Coperet C, Lesage A, Emsley L. J Am Chem Soc. 2014; 136:2324–2334. [PubMed: 24410528]
37. Pines A, Waugh JS, Gibby MG. J Chem Phys. 1972; 56:1776–1777.
38. Vold RL, Waugh JS, Klein MP, Phelps DE. J Chem Phys. 1968; 48:3831–3832.
39. Freeman R, Hill HDW. J Chem Phys. 1971; 54:3367–3377.
40. Bennett AE, Rienstra CM, Auger M, Lakshmi KV, Griffin RG. J Chem Phys. 1995; 103:6951–6958.
41. Derollez P, Dudognon E, Affouard F, Danede F, Correia NT, Descamps M. Acta Crystallographica Section B. 2010; 66:76–80.
42. Mahieu A, Willart J-f, Dudognon E, Eddleston MD, Jones W, Danède F, Descamps M. Journal of pharmaceutical sciences. 2013; 102:462–468. [PubMed: 23132509]
43. Balendiran GK, Rath N, Kotheimer A, Miller C, Zeller M, Rath NP. Journal of pharmaceutical sciences. 2012; 101:1555–1569. [PubMed: 22246648]
44. Surwase SA, Boetker JP, Saville D, Boyd BJ, Gordon KC, Peltonen L, Strachan CJ. Molecular Pharmaceutics. 2013; 10:4472–4480. [PubMed: 24025118]
45. Bradley, JP. PhD. University of Warwick; 2011.
46. Levine SG, Hicks RE, Gottlieb HE, Wenkert E. J Org Chem. 1975; 40:2540–2542. [PubMed: 1165512]
47. Simpson TJ, Holker JSE. Phytochemistry. 1977; 16:229–233.

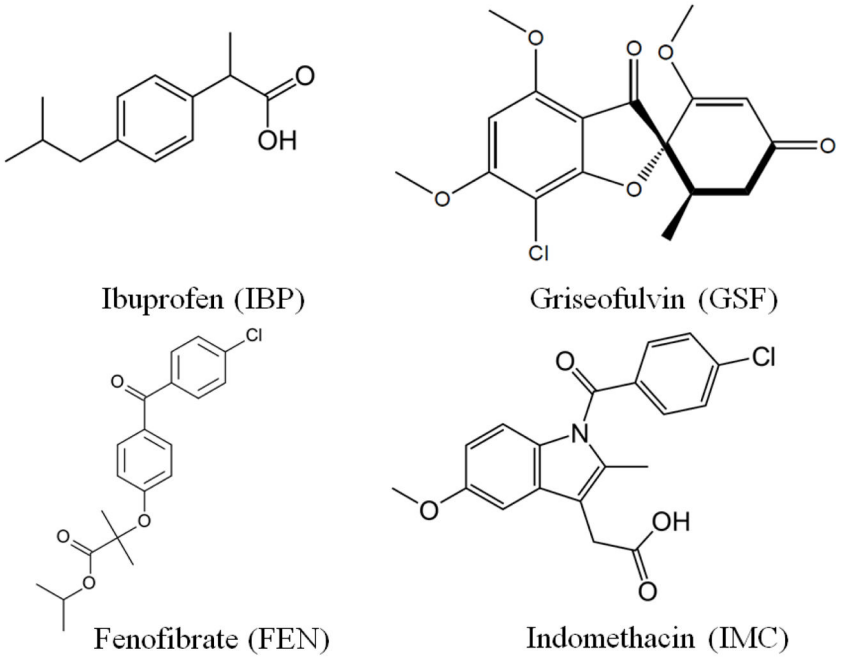

Figure 1.
Organic compounds of interest for API loading in porous silica used within this study.

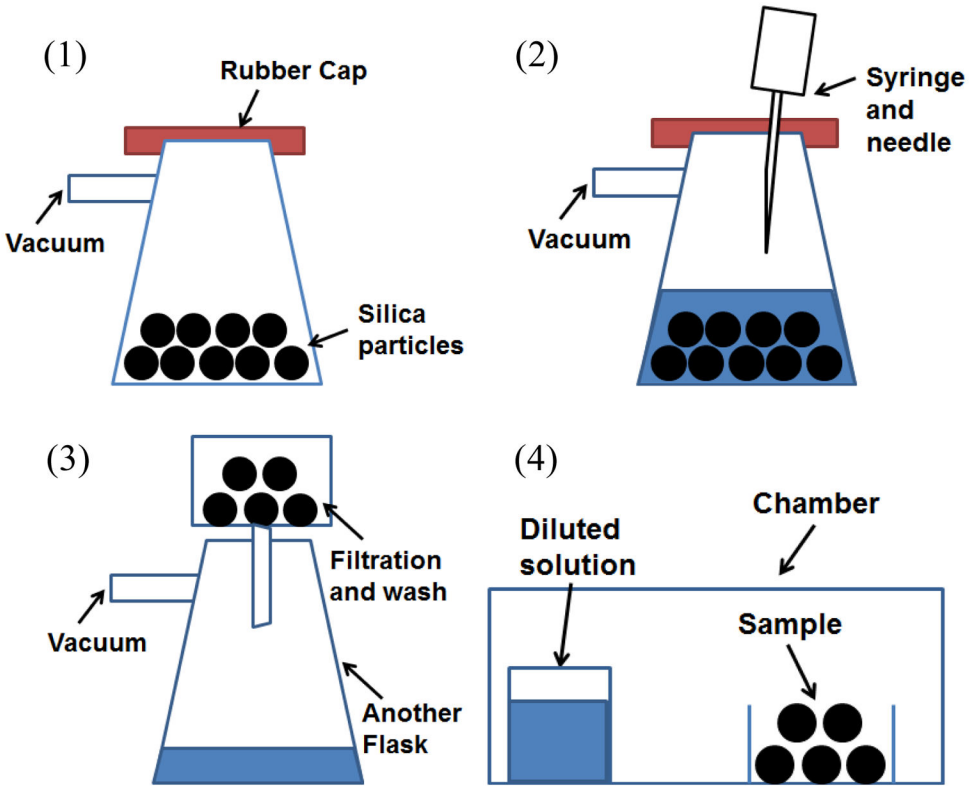

Figure 2.
Four step loading procedure of impregnating porous particles with API solutions under low pressure.

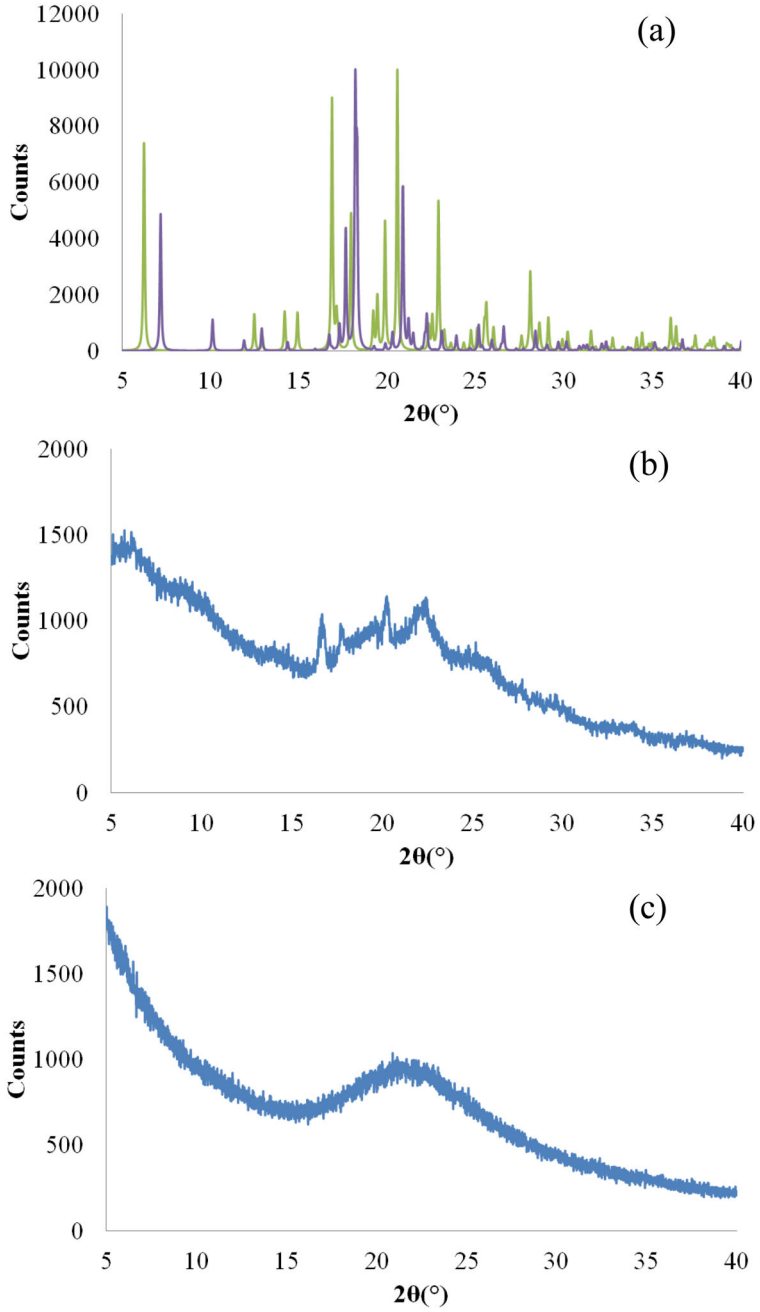

Figure 3.

XRPD patterns of prepared IBP samples. Reference X-ray diffraction data for form I (green) and II (purple) are presented in (a), IBP loaded in ~ 40 nm porous silica particles of light- (b) and medium-wash (c). Characteristic peaks in (b) match well with form I (a), showing crystals on the surface and within a few micrometers below the surface of light-wash treatment are form I.

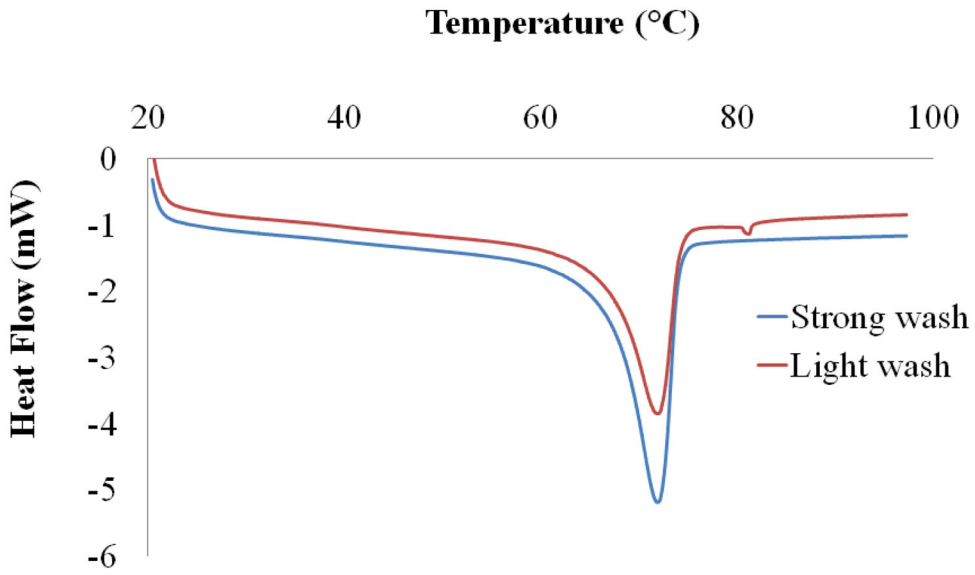

Figure 4.

DSC results of FEN loaded in porous silica particles of ~ 40 nm pores of light- (red) and strong-wash (blue). Samples of light wash show two peaks (71.4 and 81.2 °C) while samples of strong wash has only one peak of 71.7 °C.

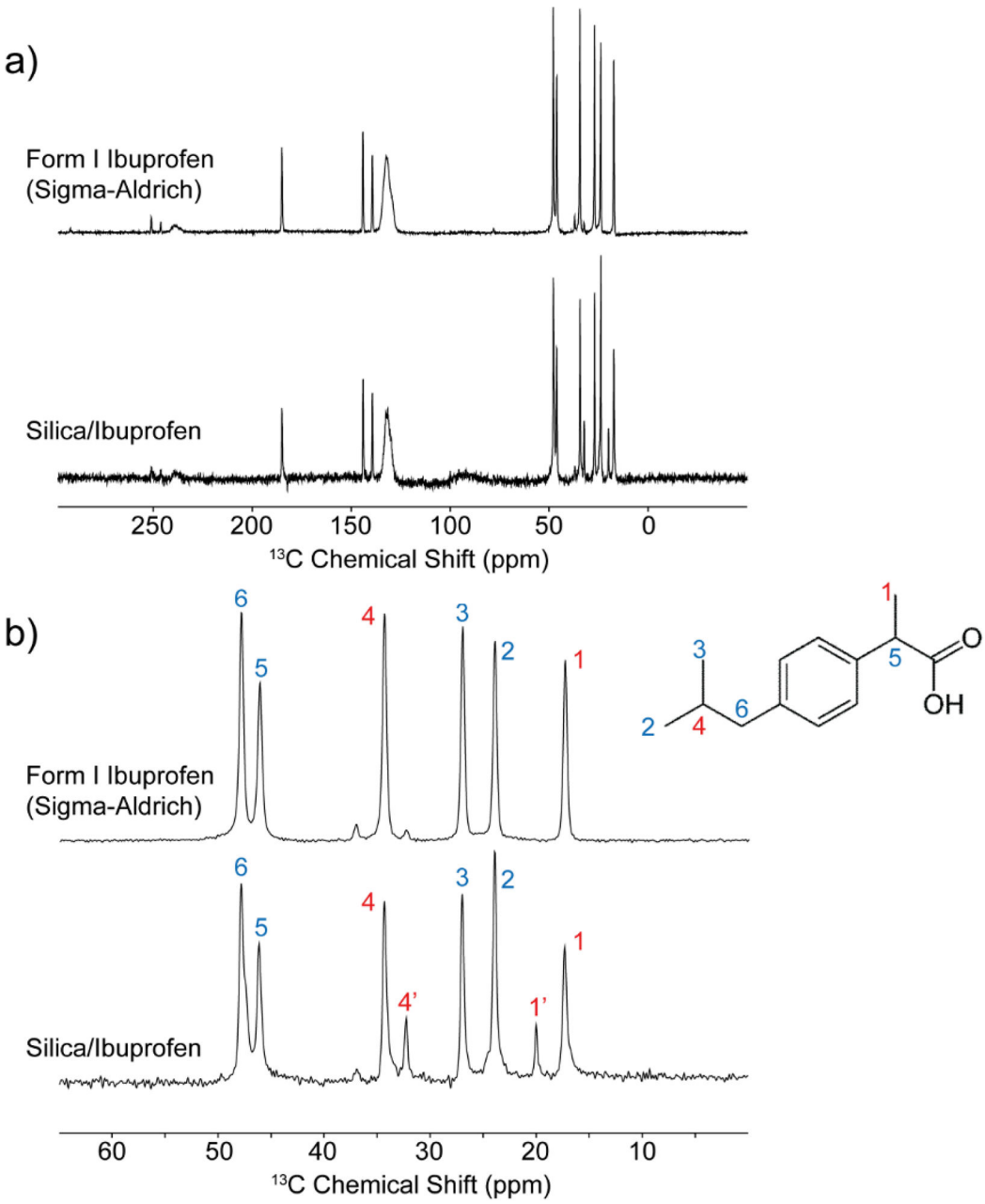

Figure 5.

^{13}C CPMAS spectra of form I IBP and silica-IBP, a) full spectra and b) expanded spectra (with ^{13}C-δ_{iso}/ppm assignment) of the aliphatic carbon region, which clearly shows the onset of additional peaks for silica-IBP (peak 1′ and 4′). The ratio of the two forms is 79:21 (Form I:unknown form).

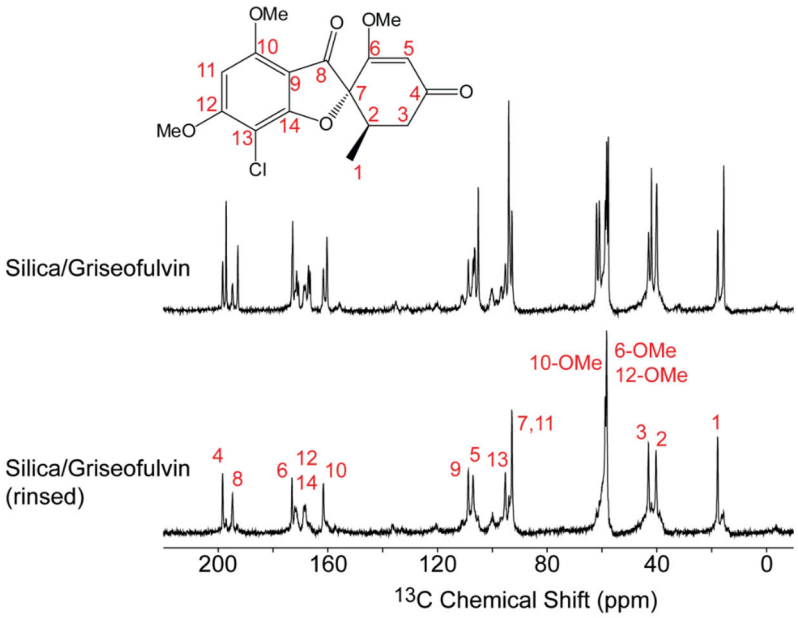

Figure 6.

^{13}C CPMAS spectra of silica-GSF before (light wash) and after (strong wash) rinsing with dichloromethane. The sharp peaks indicate the presence of crystalline polymorphs and the line broadening at the base suggests amorphous content. Strong washing (bottom spectrum) removed the surface polymorph, while the pore polymorph and amorphous phases remain. A detailed comparison can be found in SI.

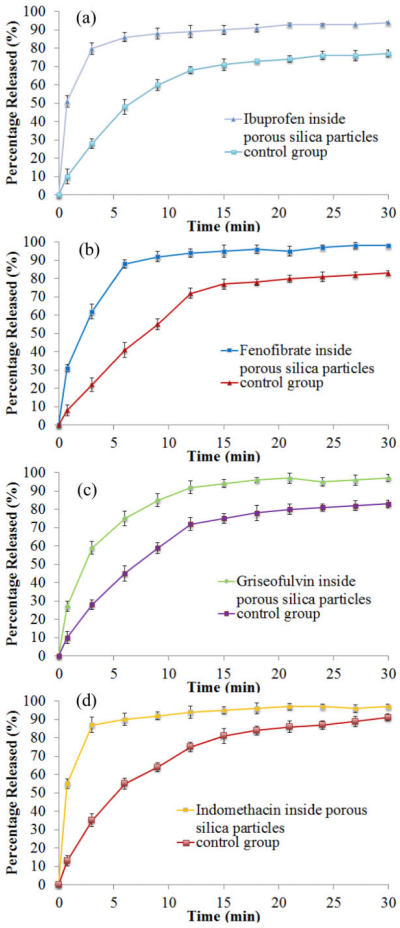

Figure 7.

Dissolution profiles of API's loaded in ~40 nm porous silica particles: (a) IBP with medium wash; (b) FEN with strong wash; (c) GSF with strong wash; (d) IMC with strong wash.

Table 1

IBP loaded in porous silica particles

Washing levels	IBP mass loaded wt %	Melting points by DSC °C	Polymorphic outcome by XRPD	Polymorphic outcome by ssNMR
No wash	28.2 ± 3.1	65.8 ± 0.2 / 75.1 ± 0.1	Form I	-
Light wash	21.7 ± 4.7	65.6 ± 0.3 / 75.0 ± 0.3	Form I	-
Medium wash	12.3 ± 2.1	65.5 ± 0.3	No crystalline peaks	79:21 (I:unknown form)
Strong wash	6.8 ± 3.0	66.0 ± 0.2	No crystalline peaks	-

Table 2

FEN loaded in porous silica particles

Washing levels	FEN mass loaded wt %	Melting points by DSC °C	Polymorphic outcome by XRPD	Polymorphic outcome by ssNMR
Light wash	15.8 ± 4.4	71.3 ± 0.3 / 81.0 ± 0.1	Form I	-
Strong wash	8.1 ± 3.5	71.2 ± 0.4	No crystalline peaks	Form I

Table 3

GSF loaded in porous silica particles

Washing levels	GSF mass loaded wt %	Melting points by DSC °C	Polymorphic outcome by XRPD	Polymorphic outcome by ssNMR
Light wash	17.2 ± 2.5	215.1 ± 0.3 / 221.3 ± 0.1	Form I	Two forms & amorphous
Strong wash	8.3 ± 2.8	205.3 ± 0.4 / 215.2 ± 0.2	No crystalline peaks	Two forms & amorphous

Table 4

IMC loaded in porous silica particles

Washing levels	IMC mass loaded wt %	Melting points by DSC °C	Polymorphic outcome by XRPD	Polymorphic outcome by ssNMR
Strong wash	9.1 ± 2.7	No peaks	No crystalline peaks	amorphous